Atmos. Chem. Phys. Discuss., 12, 26843–26869, 2012
www.atmos-chem-phys-discuss.net/12/26843/2012/
doi:10.5194/acpd-12-26843-2012

Atmospheric Chemistry and Physics Discussions

Airborne high spectral resolution lidar observation of pollution aerosol during EUCAARI-LONGREX

S. Groß[1], M. Esselborn[1,*], F. Abicht[1,], M. Wirth[1], A. Fix[1], and A. Minikin[1]**

[1]Deutsches Zentrum für Luft- und Raumfahrt (DLR), Institut für Physik der Atmosphäre (IPA), Münchner Str. 20, Oberpfaffenhofen, 82234 Weßling, Germany
[*]now at: European Southern Observatory, Karl-Schwarzschild-Str. 2, 85748 Garching, Germany
[**]now at: Max-Born-Institut, Max-Born-Str. 2a, 12489 Berlin, Germany

Received: 12 July 2012 – Accepted: 26 September 2012 – Published: 11 October 2012

Correspondence to: S. Groß (silke.gross@dlr.de)

Published by Copernicus Publications on behalf of the European Geosciences Union.

Abstract

Airborne high spectral resolution lidar observations over Europe during the EUCAARI field experiment in May 2008 are analysed with respect to spatial distribution and optical properties of continental pollution aerosol. Continental aerosol is characterized by its depolarisation and lidar ratio. Mean values of 6 % ± 1 % for the particle linear depolarisation ratio, and 56 sr ± 6 sr for the lidar ratio were found for pollution aerosol. Both, lidar ratio and depolarisation ratio at 532 nm show virtually no variations for all analysed days during the measurement campaign.

1 Introduction

Aerosol particles are a main component of the atmosphere and affect the Earth's climate system in two different ways. They scatter and absorb the solar and terrestrial radiation, and they act as cloud condensation nuclei and for this reason influence cloud properties. According to the findings of the IPCC (Foster et al., 2007) the current level of scientific understanding of the impact of aerosols on the global climate system is considered as medium to low. The effect of aerosols depends on the spatial and vertical distribution of aerosols, on their chemical and microphysical properties, as well as on the reflectance of the underlying surface and the presence of clouds. As aerosols show a large spatial and temporal variability their impact on regional scale can be quite different (IPCC, 2007). To improve our knowledge on the impact of aerosols on the Earth's climate system, long-term observations and coordinated observations during intensive field campaigns (such as closure studies, Quinn et al., 1996) are crucial. Furthermore, the presence of aerosols in the lower atmosphere plays a significant role in air quality and health considerations.

The EUCAARI (European integrated project on Aerosol Cloud Climate and Air Quality Interactions) project is part of the 6th framework program of the European Commission and aims to investigate the role of aerosols on climate and air quality

ACPD
12, 26843–26869, 2012

(Kulmala et al., 2009). Embedded in the EUCAARI intensive observational period, the aircraft field experiment EUCAARI-LONGREX (Long Range Experiment) was conducted in May/June 2008 to investigate physical and chemical properties of atmospheric aerosols within the free troposphere and the boundary layer on European scale. Essential activities of this experiment included a comprehensive characterization of main aerosol types over Europe and their exchange between boundary layer and free troposphere. Spatial and temporal gradients of aerosol loading were investigated to evaluate aerosol sources and sinks. Moreover, the experiment included a closure study of aerosol optical thickness observed from ground, sky and space. During EUCAARI-LONGREX two research aircraft were based at the airport of Oberpfaffenhofen, Germany. The Falcon 20 jet, operated by the German Aerospace Centre (DLR), equipped with a nadir viewing HSRL (High Spectral Resolution Lidar) and a comprehensive in-situ instrumentation generally focused on the upper troposphere and occasionally guided the low flying British BAe-146 (FAAM, Facility for Airborne Atmospheric Measurements) into specific aerosol layers. Above ground observation sites and other regions of particular interest the Falcon flew stacked vertical profiles in order to sample the atmospheric column from high altitude down to the boundary layer.

Airborne lidar instruments are particularly suitable to observe both, the horizontal and the vertical distribution of aerosol structures on a regional scale. The advantage of HSRL over normal backscatter lidar is the ability to directly measure the extinction-to-backscatter ratio (lidar ratio) of aerosols (Shipley et al., 1983; Shimizu et al., 1983). The value of this quantity depends on the physical properties of aerosols, namely the size distribution, the complex index of refraction and the morphology (Evans, 1988). It does not depend on its concentration. Previous studies show that the lidar ratio is a suitable measure to classify different types of aerosol (Müller et al., 2007; Mattis et al., 2004). Currant spaceborne lidars such as the Cloud Aerosol Lidar and Infrared Pathfinder Satellite Observation (CALIPSO) instrument (Winker et al., 2007) measure the attenuated backscatter signal on a global scale. The retrieval of vertical aerosol extinction profiles relies on a-priori assumptions on the lidar ratio. Therefore, the accuracy

ACPD
12, 26843–26869, 2012

of the retrieved extinction profile is determined by the assumed lidar ratio. The results of airborne HSRL measurements can be helpful to improve the informative value of spaceborne measurements. This paper focuses on the analysis of the airborne HSRL measurements of the aerosol lidar ratio and the particle linear depolarisation ratio taken during the first half of EUCAARI-LONGREX (6 May to 14 May). Both quantities only depend on the particle properties of the aerosol type and can be used to classify different types of aerosol.

2 Methods

2.1 DLR Falcon HSRL

During the EUCAARI-LONGREX field campaign a HSRL system was operated on board the DLR Falcon research aircraft. This system originally has been developed as an airborne demonstrator for a possible future spaceborne multi-wavelength differential absorption lidar (DIAL) for water vapour measurements at 935 nm (WALES – Wirth et al., 2009). In addition to the H_2O-channels the system provides backscatter and depolarisation channels at 1064 nm and 532 nm for aerosol characterization. At 532 nm a molecular channel is implemented for the HSRL measurements. The HSRL receiver channel was already successfully deployed during former field campaigns. A detailed technical description of the HSRL system and a presentation of its measurements can be found in Esselborn et al. (2008) and Esselborn et al. (2009). Typically, the system allows signal integration times as short as a few seconds with an acceptable statistical error of less than 5 % in the backscatter data. The vertical resolution of the profiles is 15 m for all backscatter and depolarisation data. For the extinction and lidar ratio profiles the vertical resolution is 360 m–700 m which is due to the necessary numerical differentiation of the extinction retrieval. Relative systematic errors of the backscatter measurements are typically 4 % to 8 %, statistical errors are typically < 1 % and therefore negligible. For the extinction measurements the relative systematic errors are

ACPD
12, 26843–26869, 2012

usually less than 5 %, so that statistical errors of typically 5 % to 20 % are dominant. Relative systematic errors of the depolarisation measurements are primarily due to mechanical accuracy of the calibration measurement and result in a relative error of the particle linear depolarisation ratio of the order of 10 % to 16 % (Esselborn et al., 2008). Because of eye safety regulations in the considerably frequented airspace over Europe, HSRL measurements at 532 nm were restricted to places which were cleared by air traffic control.

2.2 Meteorological conditions during EUCAARI

The synoptic situation of the first half of the EUCAARI-LONGREX field campaign, from 6–14 May 2008, was dominated by a persistent high-pressure blocking system, remaining almost stationary over Southern Sweden and Denmark (Fig. 1). Due to the stability of the system during the main part of the campaign, a constant east-west transport of air-mass could be observed in Central Europe. The absence of precipitation during this period favoured the accumulation of pollution aerosol in the continental boundary layer. Figure 1 shows the typical meteorological situation during the first half of the campaign exemplarily for the geopotential and wind at 850 hPa on 10 May 2008.

From 11 May to 14 May the high-pressure system moved westward, north-east of the British Islands and started to decay on 14 May. The second half of the field campaign was characterized by an undefined advection mostly from northerly directions. A detailed description of the meteorological situation during the EUCAARI-LONGREX campaign can be found in Hamburger et al. (2011).

Figure 2 shows a backward trajectory analysis for the five Falcon flight missions during the first half of the field campaign. The backward trajectories show a circulated flow pattern and advection from eastern directions. The trajectories were calculated with the Hybrid Single Particle Lagrangian Integrated Trajectory (HYSPLIT) model (Draxler and Rolph, 2012) and the NCEP Global Data Assimilation System (GDAS) data, and start at the times and places the HSRL measurements were analysed. The duration is five days backward for all trajectories.

ACPD
12, 26843–26869, 2012

2.3 Flight missions during EUCAARI

A total of 48 flight hours were performed during 14 flight missions (Hamburger et al., 2011). Due to the persistent high pressure system transporting air masses in westerly directions, the flights were restricted to areas north of the Alps. Figure 3 shows a compilation of all Falcon flight missions performed during EUCAARI-LONGREX.

During EUCAARI-LONGREX the German Falcon operated out of Oberpfaffenhofen airport (48.08 N, 11.29 W). The flight patterns of the Falcon were designed for lidar observation at high altitude and subsequent in situ profiling over the instrumented ground stations and other specific regions identified by lidar.

3 Results and discussion

Due to the meteorological conditions, only measurements during the first half of the campaign are used for the characterization of pollution aerosols. This restriction is necessary to make sure that pollution aerosol was the dominant, if not the only aerosol type within the observed aerosol layers, and to ensure high aerosol load within these aerosol layers to achieve high accurate measurements with resulting small uncertainties. We present a case study on 14 May 2008 to exemplarily show an analysis of the used measurement data. This day was chosen, as extensive data analyses in terms of a closure study are available for that day, i.e. lidar measurements, vertical profiling of in-situ measurements, and satellite (PARASOL) overpass (Kulmala et al., 2011).

3.1 Case study of pollution aerosol on 14 May 2008

The flight mission on 14 May 2008 was dedicated to coordinated observations of a pollution aerosol plume west of Ireland. To ensure maximum flight endurance west of the coast of Ireland the Falcon aircraft was transferred to Shannon/Ireland the day before and performed a local flight on 14 May 2008. (The Falcon flight track is shown in Fig. 3 in the yellow line.) The location west of the Irish coast was chosen due to a forecasted

ACPD
12, 26843–26869, 2012

pollution transport event. Backward trajectories (Fig. 2 red line) show, that the observed air masses were transported from western directions, and crossed Northern Germany, the Netherlands, Southern England and Southern Ireland on their way. The mean flight altitude during this flight leg was 10 km. The colour coding in Fig. 4 indicates the aerosol optical depth (AOD) between flight altitude and ground along the flight track. The AOD ranged between ∼0.1 near the Ireland Coast and ∼0.5. The AOD was significantly higher in the south-eastern part of the flight leg.

The lidar backscatter ratio (Fig. 5) indicated the aerosol layers along the flight path, in the marine boundary layer and in the free troposphere up to about 4.5 km altitude. The aerosol structure was inhomogeneous with several elevated layers.

In order to allow the analysis of air masses of pure continental origin having not being influenced by marine boundary layer and/or advection the HSRL data was filtered according to the following criteria:

1. The residence time of the aerosol over the European Continent without Scandinavia is larger than 36 h.
2. During these 36 h the trajectories stayed below 2.5 km (750 hPa).
3. During the last 12 h before measurements the trajectories have been above 0.8 km (930 hPa) over the ocean.

Furthermore, we choose measurement periods with sufficient aerosol load and vertical homogeneity of the layering to avoid uncertainties due to inhomogeneity in the averaged data. Accordingly, a part in the middle of the flight region was chosen for a detailed study, which is indicated in Fig. 5 by the red rectangle. The mean profiles of the particle backscatter coefficient, the particle extinction coefficient, the particle lidar ratio and the particle linear depolarisation ratio are shown in Fig. 6.

From these profiles, a two layer structure of the selected time period is observable. The lower layer reaches up to about 1.4 km and shows a mean lidar ratio of 60 sr and a mean particle linear depolarisation ratio of about 5 %, the upper layer (from

ACPD
12, 26843–26869, 2012

about 1.7 km to 2.5 km) shows a mean lidar ratio of about 67 sr and a mean value of the particle linear depolarisation ratio of about 6 %. The mean particle extinction coefficient in the lower layer is about 0.2 km^{-1}, whereas the maximum value of the particle extinction coefficient in the upper layer is only 0.1 km^{-1}. The latter results are in very good agreement with the vertical profiles of the extinction coefficient derived from the in situ particle size distribution measurements on board the Falcon aircraft (Kulmala et al., 2011).

3.2 General findings of all pollution cases

In the previous subsection we presented an analysis of the case study on 14 May 2008 as an example. Now we consider all analysed lidar measurements of pollution cases during the first half of the EUCAARI-LONGREX campaign. To get an overview of the temporal and spatial distribution of the pollution aerosols Fig. 7 shows vertical profiles of the backscatter coefficient, the extinction coefficient, the lidar ratio and the particle linear depolarisation ratio (all at 532 nm) for the remaining four HSRL measurements. The profiles correspond to measurements at the south-eastern coast of England on 6 May (11:02 UTC), near Melpitz, Germany, on 6 May (16:08 UTC), near Cabauw, Netherlands, on 8 May (14:45 UTC), and near Cottbus, Germany, on 13 May (11:24 UTC). The backscatter coefficient for these measurements ranged between about 0.001 $km^{-1}\,sr^{-1}$ to about 0.002 $km^{-1}\,sr^{-1}$ within the pollution layers. The corresponding extinction coefficient in the pollution layer was about 0.1 km^{-1}. The lidar ratio of pollution aerosol ranged between 33 sr and 77 sr, and the particle linear depolarisation ratio showed values between 3 % and 11 %.

As the lidar ratio and the particle linear depolarisation ratio are intensive aerosol properties, i.e. they are only dependent on the aerosol type and not on the aerosol concentration; we will have a closer look on these two aerosol properties. Lidar ratio and particle linear depolarisation ratio information for the different considered days, as well as information on the considered height level and measurement location are summarised in Table 1. Regarding all measurements included into this study, the mean

ACPD
12, 26843–26869, 2012

lidar ratio is 56 sr ± 6 sr. The mean particle linear depolarisation ratio is 6 % ± 1 %. The ±-values indicate the standard deviation including all selected measurements. Figure 8 shows the lidar ratio plotted against the particle linear depolarisation ratio for selected flight tracks according to the trajectory criteria described above. The grey dots show the results of all measurement points considered as pollution aerosols. The mean values of lidar ratio and particle linear depolarisation ratio within the pollution layers of the vertical profiles (Figs. 6 and 7) are colour-coded corresponding to the trajectories shown in Fig. 2. Although the measurements were performed at different places over Europe and at different times during the first half of the campaign, the lidar ratio and particle linear depolarisation ratio of the different measurements show no variation for pollution aerosol particles within the measurement accuracy (Fig. 8 and Table 1).

Figure 9 shows the histograms of the observed lidar ratio and the particle linear depolarisation ratio, respectively. Regarding all considered measurements during the first half of the EUCAARI-LONGREX campaign, a lidar ratio between 50 sr and 65 sr is observed at about 75 % of the measurement points. The median is 56 sr. Lidar ratios around and below 40 sr, found for about 5 % of all measurement points, may indicate rural particles (Evans, 1988; Anderson et al., 2000) or aerosol mixtures.

For the particle linear depolarisation ratio about 40 % of all measurement points show values between 5 % and 6 %, and about 75 % of all measurement points show values between 4 % and 7 %. The median is 6 %.

But not only the lidar ratio and the particle linear depolarisation ratio are only dependent on the aerosol type. Also the colour ratio, i.e. the ratio of the particle backscatter coefficients at 532 nm and at 1064 nm, is independent of the aerosol concentration. It provides information about the particle size. Colour ratios around one indicate large particles, while colour ratios around two and higher are an indication for small particles compared to the lidar wavelength. For the layers of pollution aerosol observed during the first half of the EUCAARI-LONGREX campaign, a mean colour ratio of 2.4 was found, indicating small, submicron particles. More than 85 % of all data points show

ACPD
12, 26843–26869, 2012

a colour ratio between 2.0 and 2.8, and less than 3.7 % show colour ratios lower than 2.0 (see Fig. 10), an indication that no large particles were present.

3.3 Discussion

The characterization of polluted air masses is an active research topic concerning air quality and climate effect. Therefore a number of papers report about measurements within polluted air masses. Lidar ratios of pollution aerosols over Central Europe were reported by Wandinger et al. (2002). They found values of 50 sr–65 sr at 532 nm from Raman lidar measurements. Ansmann et al. (2000) found lidar ratios of 60 sr–90 sr in polluted aerosol layers over India, measured with a Raman lidar system during the field campaign INDOEX. Müller et al. (2001) reported about mean lidar ratios of about 60 sr for the same measurement experiment. During the ACE-2 field campaign Raman lidar measurements in polluted aerosol layers over Portugal showed lidar ratios of 50 sr–70 sr (Ansmann et al., 2001). Xie et al. (2008) found values of 61 sr ± 14 sr in moderately polluted aerosol layers over Beijing, China. Using a 180° backscatter nephelometer lidar ratios of 64 sr ± 4 sr for pollution aerosol over Illinois (Anderson et al., 2000), and 60 sr–70 sr for continental aerosols were observed (Doherty et al., 1999). Inversions from AERONET (Holben et al., 1998) sun-photometer measurements resulted in values of 71 sr ± 10 sr for industrial pollution over Europe, and over Middle and North America (Cattrall et al., 2005). Measurements over South-East Asia resulted in values of 58 sr ± 10 sr for industrial pollution aerosols (Cattrall et al., 2005). While a number of papers deal with the lidar ratio of industrial pollution or urban haze, measurements of the particle linear depolarisation ratio of this aerosol type are rare. Müller et al. (2007) reported about particle linear depolarisation ratios for urban haze of about or lower 5 % over Central and South-West Europe, and over North America. Burton et al. (2012) found values between 2–11 %. In polluted air masses over Beijing, China, mean values of the particle linear depolarisation ratio of 7 % were found (Xie et al., 2008). Our values of 56 sr ± 6 sr and 6 % ± 1 % for pollution aerosols agree well with former findings. Considering the uncertainties of the different measurements, neither in the lidar ratio

ACPD
12, 26843–26869, 2012

nor in the particle linear depolarization ratio a dependence on measurement location and measurement time is obvious.

The meteorological conditions and the flight strategy during EUCAARI-LONGREX were best suited to study pollution aerosols with respect to location and age of the aerosols. Airborne HSRL measurements are an excellent tool to characterize aerosols, as they provide high-resolved temporal and vertical information on the aerosol distribution and optical properties with high accuracy. During all measurements included into this study, pollution aerosols over and from different locations across Europe and of different age could be observed. Even with the high accuracy of our lidar measurements, no differentiation of pollution aerosols from different origin and age was possible. Also no significant differences of the observed optical properties to former findings could be found. This is in particular valuable to define the aerosol type "pollution aerosol", and to determine the right input parameter for aerosol retrievals, e.g. of satellite instruments such as CALIOP. Furthermore, the characterization of the aerosol type "pollution aerosol" is valuable to distinguish pollution aerosol from other aerosol types and to determine mixtures with other types of aerosols, as it is most probably the case for the measurements on 6 May – 11:02 UTC north-east of the English coast and on 14 May south-west of the Irish coast. On both days the values of the lidar ratio decrease with decreasing height (below about 1 km). This is an indication for the mixture with marine aerosols, which have similar values for the particle linear depolarisation ratio, but lower values (of about 18 sr – Groß et al., 2011) for the lidar ratio.

4 Conclusions

During the EUCAARI-LONGREX field campaign airborne HSRL observations were performed over Europe to characterize the optical properties and the spatial distribution of pollution aerosol.

A total of 14 Falcon flight missions including 48 flight hours were performed. The meteorological conditions were determined by a persistent high pressure system over

ACPD
12, 26843–26869, 2012

the North Sea during the first half of the observing period and a northerly advection during the second half. Especially during the first half high AOD values have been observed due to the build-up of a pollution layer in the absence of precipitation.

The main goal of this study was to determine lidar derived optical properties for European pollution aerosols. From all flight missions 5 flight legs were selected during which mainly continental pollution aerosol has been observed. The selection was made on the basis of backward trajectory analysis. The mean lidar ratio of the pollution aerosol is 56 sr ± 6 sr. The mean depolarisation ratio is 6 % ± 1 %. The characteristic quantities determined by HSRL such as the lidar ratio and the depolarisation ratio of the aerosol show virtually no dependency on the location of the measurement or on the age of the aerosol plumes. This is in particular valuable to define an aerosol type "pollution aerosol" and to distinguish it from other aerosol types. The possibility to classify different aerosol types by means of lidar derived optical properties is subject of further research work (Groß et al., 2012).

Acknowledgements. This work has been partly funded by EUCAARI (European Integrated project on Aerosol Cloud Climate and Air Quality interactions) N0. 036833-2, and by HALO-SPP NO. 1294/2. The authors like to thank the staff members of the DLR Falcon 20 from the DLR Flight operation department during the EUCAARI-LONGREX campaign. Especially, we want to thank Thomas Hamburger for the help with the meteorological description.

References

Anderson, T. L., Masonis, S. J., Covert, D. S., Charlson, R. J., and Rood, M. J.: In situ measurement of the aerosol extinction-to-backscatter ratio at a polluted continental site, J. Geophys. Res., 105, 26907–26915, doi:10.1029/2000JD900400, 2000.

Ansmann, A., Althausen, D., Wandinger, U., Franke, K., Müller, D., Wagner, F., and Heintzenberg, J.: Vertical profiling of the indian aerosol plume with six-wavelength lidar during indoex: a first case study, Geophys. Res. Lett., 27, 963–966, doi:10.1029/1999GL010902, 2000.

ACPD

12, 26843–26869, 2012

Ansmann, A., Wagner, F., Althausen, D., Müller, D., Herber, A., and Wandinger, U.: European pollution outbreaks during ace 2: lofted aerosol plumes observed with raman lidar at the portuguese coast, J. Geophys. Res., 106, 20725–20733, doi:10.1029/2000JD000091, 2001.
Burton, S. P., Ferrare, R. A., Hostetler, C. A., Hair, J. W., Rogers, R. R., Obland, M. D., Butler, C. F., Cook, A. L., Harper, D. B., and Froyd, K. D.: Aerosol classification using airborne High Spectral Resolution Lidar measurements – methodology and examples, Atmos. Meas. Tech., 5, 73–98, doi:10.5194/amt-5-73-2012, 2012.
Cattrall, C., Reagan, J., Thome, K., and Dubovik, O.: Variability of aerosol and spectral lidar and backscatter and extinction ratios of key aerosol types derived from selected aerosol robotic network locations, J. Geophys. Res., 110, D10S11, doi:10.1029/2004JD005124, 2005.
Doherty, S. J., Anderson, T. L., and Charlson, R. J.: Measurement of the lidar ratio for atmospheric aerosols with a 180 backscatter nephelometer, Appl. Optics, 38, 1823–1832, doi:10.1364/AO.38.001823, 1999.
Draxler, R. R. and Rolph, G. D.: Hysplit (hybrid single particle lagrangian integrated trajectory) model, NOAA Air Resources Laboratory, Silver Spring, MD, 2012.
Esselborn, M., Wirth, M., Fix, A., Tesche, M., and Ehret, G.: Airborne high spectral resolution lidar for measuring aerosol extinction and backscatter coefficients, Appl. Optics, 47, 346–358, doi:10.1364/AO.47.000346, 2008.
Esselborn, M., Wirth, M., Fix, A., Weinzierl, B., Rasp, K., Tesche, M., and Petzold, A.: Spatial distribution and optical properties of saharan dust observed by airborne high spectral resolution lidar during samum 2006, Tellus B, 61, 131–143, doi:10.1111/j.1600-0889.2008.00394.x, 2009.
Evans, B.: Sensitivity of the backscatter/extinction ratio to changes in aerosol properties: implications for lidar, Appl. Optics, 27, 3299–3306, doi:10.1364/AO.27.003299, 1988.
Forster, P., Ramaswamy, V., Artaxo, P., Berntsen, T., Betts, R., Fahey, D. W., Haywood, J., Lean, J., Lowe, D. C., Myhre, G., Nganga, J., Prinn, R., Raga, G., Schultz, M., and Van Dorland, R.: Changes in atmospheric constituents and in radiative forcing, in: Climate Change 2007: The Physical Science Basis, Contribution of Working Group I to the Fourth Assessment Report of the Intergovernmental Panel on Climate Change, edited by: Solomon, S., Qin, D., Manning, M., Chen, Z., Marquis, M., Averyt, K. B., Tignor, M., and Miller, H. L., Cambridge University Press, Cambridge, UK and New York, NY, USA, 129–234, 2007.
Groß, S., Tesche, M., Freudenthaler, V., Toledano, C., Wiegner, M., Ansmann, A., Althausen, D., and Seefeldner, M.: Characterization of saharan dust, marine aerosols and mixtures of

ACPD
12, 26843–26869, 2012

biomass burning aerosols and dust by means of multi-wavelength depolarization- and raman-lidar measurements during samum-2, Tellus B, 63, 706–724, doi:10.1111/j.1600-0889.2011.00556.x, 2011.

Groß, S., Esselborn, M., Weinzierl, B., Wirth, M., Fix, A., and Petzold, A.: Aerosol classification by airborne high spectral resolution lidar observations, Atmos. Chem. Phys. Discuss., 12, 25983–26028, doi:10.5194/acpd-12-25983-2012, 2012.

Hamburger, T., McMeeking, G., Minikin, A., Birmili, W., Dall'Osto, M., O'Dowd, C., Flentje, H., Henzing, B., Junninen, H., Kristensson, A., de Leeuw, G., Stohl, A., Burkhart, J. F., Coe, H., Krejci, R., and Petzold, A.: Overview of the synoptic and pollution situation over Europe during the EUCAARI-LONGREX field campaign, Atmos. Chem. Phys., 11, 1065–1082, doi:10.5194/acp-11-1065-2011, 2011.

Holben, B., Eck, T. F., Slutsker, I., Tanré, D., Buis, J. P., Setzer, A., Vermote, E., Reagan, J. A., Kaufman, Y. J., Nakajima, T., Lavenu, F., Jankowiak, I., and Smirnov, A.: Aeronet – a federated instrument network and data archive for aerosol characterization, Remote Sens. Environ., 66, 1–16, doi:10.1016/S0034-4257(98)00031-5, 1998.

Kulmala, M., Asmi, A., Lappalainen, H. K., Carslaw, K. S., Pöschl, U., Baltensperger, U., Hov, Ø., Brenquier, J.-L., Pandis, S. N., Facchini, M. C., Hansson, H.-C., Wiedensohler, A., and O'Dowd, C. D.: Introduction: European Integrated Project on Aerosol Cloud Climate and Air Quality interactions (EUCAARI) integrating aerosol research from nano to global scales, Atmos. Chem. Phys., 9, 2825–2841, doi:10.5194/acp-9-2825-2009, 2009.

Kulmala, M., Asmi, A., Lappalainen, H. K., Baltensperger, U., Brenguier, J.-L., Facchini, M. C., Hansson, H.-C., Hov, Ø., O'Dowd, C. D., Pöschl, U., Wiedensohler, A., Boers, R., Boucher, O., de Leeuw, G., Denier van der Gon, H. A. C., Feichter, J., Krejci, R., Laj, P., Lihavainen, H., Lohmann, U., McFiggans, G., Mentel, T., Pilinis, C., Riipinen, I., Schulz, M., Stohl, A., Swietlicki, E., Vignati, E., Alves, C., Amann, M., Ammann, M., Arabas, S., Artaxo, P., Baars, H., Beddows, D. C. S., Bergström, R., Beukes, J. P., Bilde, M., Burkhart, J. F., Canonaco, F., Clegg, S. L., Coe, H., Crumeyrolle, S., D'Anna, B., Decesari, S., Gilardoni, S., Fischer, M., Fjaeraa, A. M., Fountoukis, C., George, C., Gomes, L., Halloran, P., Hamburger, T., Harrison, R. M., Herrmann, H., Hoffmann, T., Hoose, C., Hu, M., Hyvärinen, A., Hõrrak, U., Iinuma, Y., Iversen, T., Josipovic, M., Kanakidou, M., Kiendler-Scharr, A., Kirkevåg, A., Kiss, G., Klimont, Z., Kolmonen, P., Komppula, M., Kristjánsson, J.-E., Laakso, L., Laaksonen, A., Labonnote, L., Lanz, V. A., Lehtinen, K. E. J., Rizzo, L. V., Makkonen, R., Manninen, H. E., McMeeking, G., Merikanto, J., Minikin, A., Mirme, S., Mor-

ACPD
12, 26843–26869, 2012

gan, W. T., Nemitz, E., O'Donnell, D., Panwar, T. S., Pawlowska, H., Petzold, A., Pienaar, J. J., Pio, C., Plass-Duelmer, C., Prévôt, A. S. H., Pryor, S., Reddington, C. L., Roberts, G., Rosenfeld, D., Schwarz, J., Seland, Ø., Sellegri, K., Shen, X. J., Shiraiwa, M., Siebert, H., Sierau, B., Simpson, D., Sun, J. Y., Topping, D., Tunved, P., Vaattovaara, P., Vakkari, V., Veefkind, J. P., Visschedijk, A., Vuollekoski, H., Vuolo, R., Wehner, B., Wildt, J., Woodward, S., Worsnop, D. R., van Zadelhoff, G.-J., Zardini, A. A., Zhang, K., van Zyl, P. G., Kerminen, V.-M., S Carslaw, K., and Pandis, S. N.: General overview: European Integrated project on Aerosol Cloud Climate and Air Quality interactions (EUCAARI) – integrating aerosol research from nano to global scales, Atmos. Chem. Phys., 11, 13061–13143, doi:10.5194/acp-11-13061-2011, 2011.

Mattis, I., Ansmann, A., Müller, D., Wandinger, U., and Althausen, D.: Multiyear aerosol observations with dualwavelength raman lidar in the framework of earlinet, J. Geophys. Res., 109, D13203, doi:10.1029/2004JD004600, 2004.

Müller, D., Wandinger, U., Althausen, D., and Fiebig, M.: Comprehensive particle characterization from three-wavelength raman-lidar observations: case study, Appl. Optics, 40, 4863–4869, doi:10.1364/AO.40.004863, 2001.

Müller, D., Ansmann, A., Mattis, I., Tesche, M., Wandinger, U., Althausen, D., and Pisani, G.: Aerosol-type-dependent lidar ratios observed with raman lidar, J. Geophys. Res., 112, D16202, doi:10.1029/2006JD008292, 2007.

Quinn, P. K., Anderson, T. L., Bates, T. S., Dlugi, R., Heintzenberg, J., von Hoyningen-Huene, W., Kulmala, M., Russel, P. B., and Swietlicki, E.: Closure in tropospheric aerosol-climate research: a review and future needs for addressing aerosol direct short-wave radiative forcing, Contributions to atmospheric physics, 69, 547–577, 1996.

Shimizu, H., Lee, S., and She, C.: High spectral resolution lidar system with atomic blocking filters for measuring atmospheric parameters, Appl. Optics, 22, 1373–1381, doi:10.1364/AO.22.001373, 1983.

Shipley, S., Tracy, D., Eloranta, E., Trauger, J., Sroga, J., Roesler, F., and Weinman, J.: High spectral resolution lidar to measure optical scattering properties of atmospheric aerosols. 1: Theory and instrumentation, Appl. Optics, 22, 3716–3724, doi:10.1364/AO.22.003716, 1983.

Wandinger, U., Müller, D., Böckmann, C., Althausen, D., Matthias, V., Bösenberg, J., Weiß, V., Fiebig, M., Wendisch, M., Stohl, A., and Ansmann, A.: Optical and microphysical character-

ACPD
12, 26843–26869, 2012

ization of biomass-burning and industrial-pollution aerosols from multiwavelength lidar and aircraft measurements, J. Geophys. Res., 117, 8125, doi:10.1029/2000JD000202, 2002.
Winker, D. M., Hunt, W. H., and McGill, M. J.: Initial performance assessment of caliop, Geophys. Res. Lett., 34, L19803, doi:10.1029/2007GL030135, 2007.
Wirth, M., Fix, A., Mahnke, P., Schwarzer, H., Schrandt, F., and Ehret, G.: The airborne multi-wavelength h2o-dial wales: system design and performance, Appl. Phys. B-Lasers O., 96, 201–213, doi:10.1007/s00340-009-3365-7, 2009.
Xie, C., Nishizawa, T., Sugimoto, N., Matsui, I., and Wang, Z.: Characteristics of aerosol optical properties in pollution and asian dust episodes over beijing, China, Appl. Optics, 47, 4945–4951, doi:10.1364/AO.47.004945, 2008.

ACPD
12, 26843–26869, 2012

Table 1. Lidar ratio (LR) and particle linear depolarisation ratio (PDR) at 532 nm, and their statistical information determined from analysed Falcon flights.

Date	Lat	Lon	Time (UTC)	Altitude Range (km)	LR mean ± std (sr)	Range (sr)	PDR mean ± std (%)	Range (%)
6 May	52.8	1.6	11:02	0.5–1.3	52 ± 6	33–69	6 ± 1	3-8
6 May	51.4	11.4	16:08	1.3–2.3	53 ± 5	40–68	6 ± 1	4–7
8 May	51.4	5.7	14:45	01.–1.3	59 ± 5	44–72	8 ± 1	6–11
13 May	51.5	13.7	11:24	1.0–2.0	52 ± 3	42–55	7 ± 1	7–10
14 May	51.5	–12.9	11:30	0.5–1.4	60 ± 5	50–70	5 ± 1	5–9
Over all					56 ± 6	33–72	6 ± 1	3–11

ACPD
12, 26843–26869, 2012

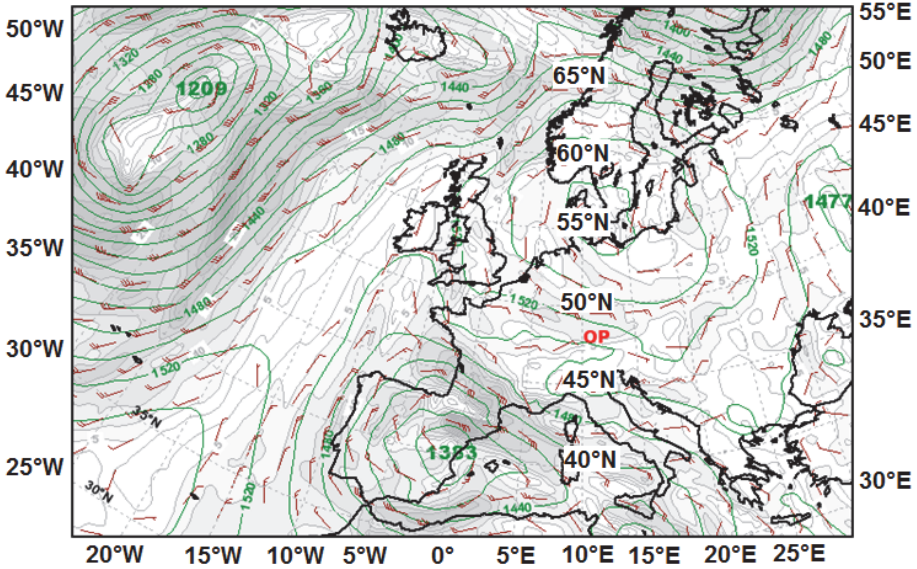

Fig. 1. Geopotential and wind field at 850 hPa on 10 May 2008. OP marks the airport of Oberpfaffenhofen.

ACPD
12, 26843–26869, 2012

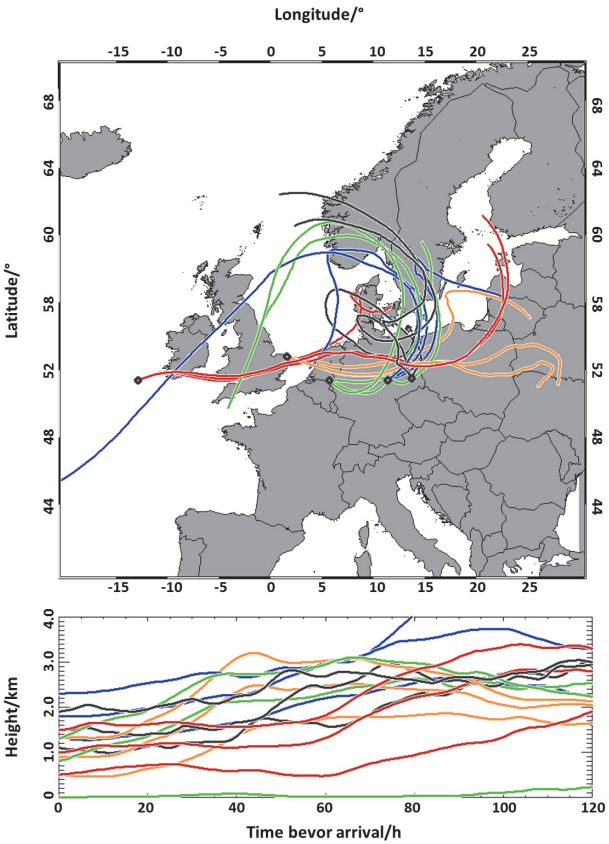

Fig. 2. 5-day backward trajectories for the locations of flight missions during the first half of the EUCAARI-LONGREX field campaign. The trajectories start in height levels identified by the lidar measurements and considered as pollution aerosols (see Table 1).

ACPD
12, 26843–26869, 2012

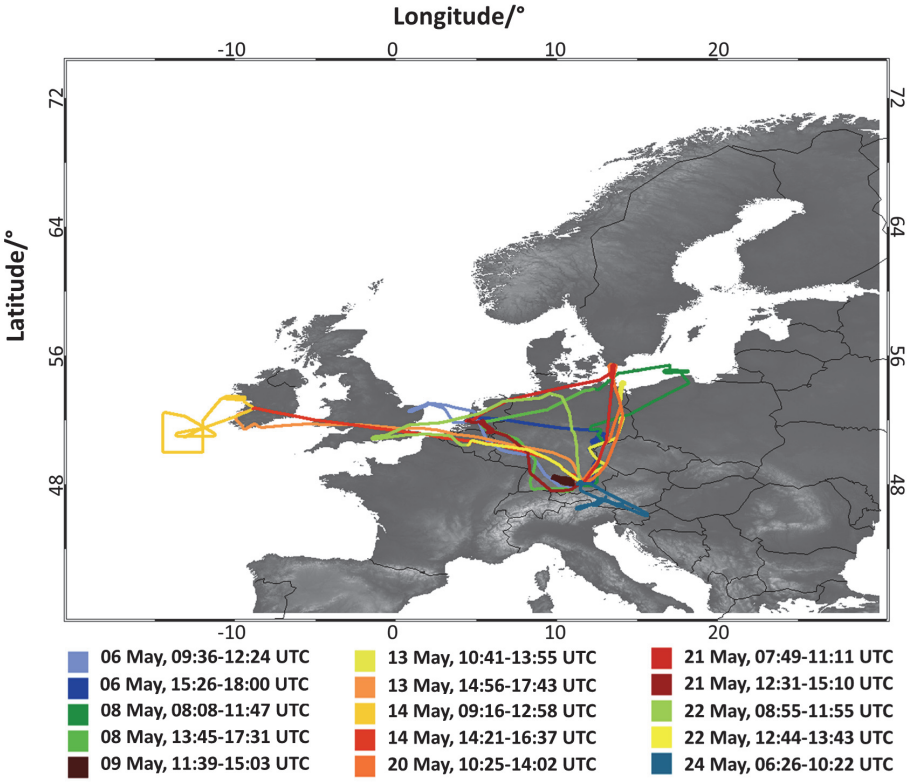

Fig. 3. Falcon flight tracks during EUCAARI-LONGREX.

ACPD
12, 26843–26869, 2012

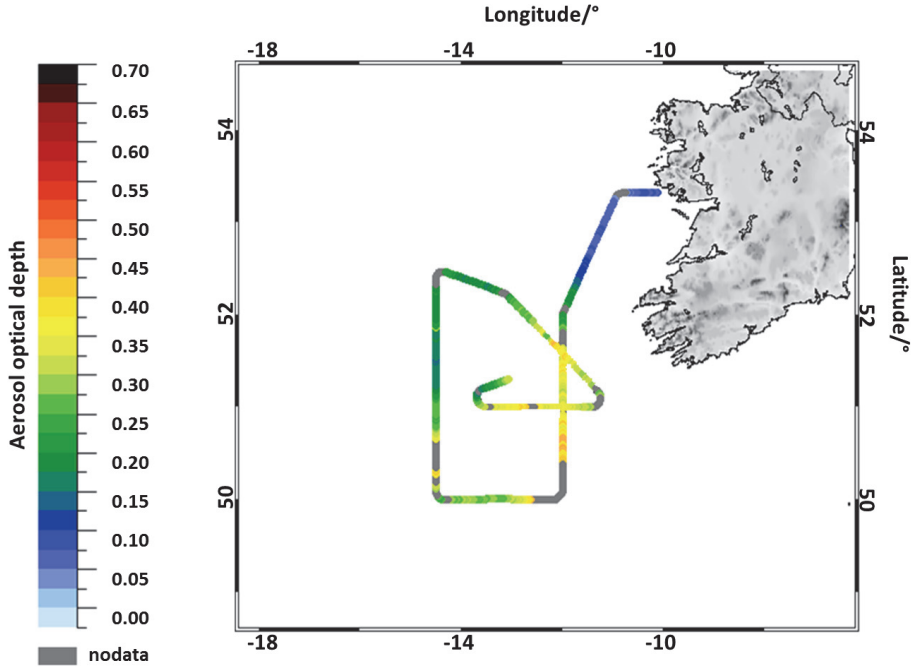

Fig. 4. AOD at 532 nm along the Falcon flight track south-west of Ireland on 14 May 2008. "nodata" marks areas in which the calculation of AOD was prevented by clouds, or by biased measurements caused by spiralling.

ACPD
12, 26843–26869, 2012

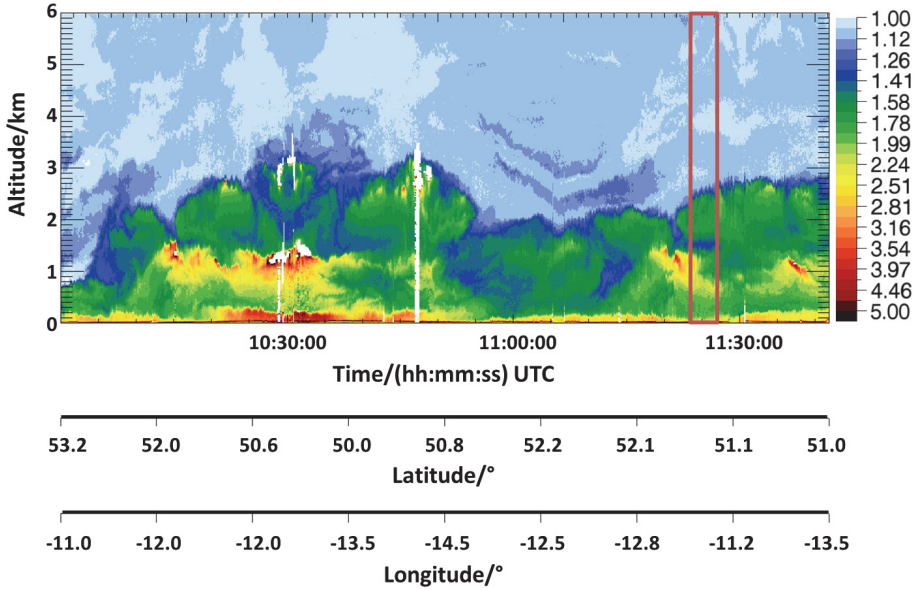

Fig. 5. Aerosol distribution shown as cross-section of the backscatter ratio at 532 nm along the flight track on 14 May 2008 shown in Fig. 4.

ACPD
12, 26843–26869, 2012

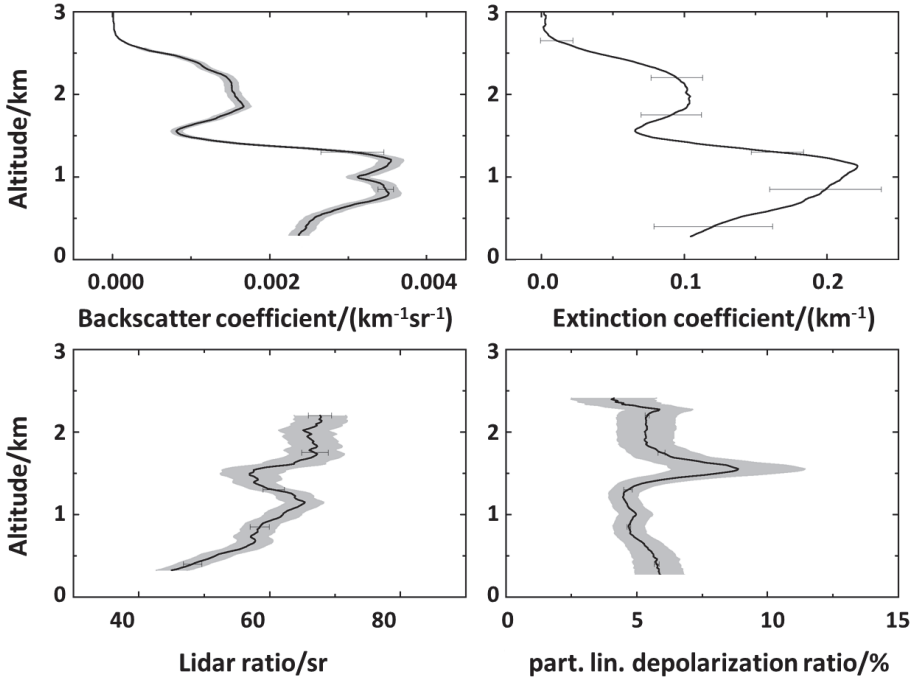

Fig. 6. HSRL profiles of particle backscatter coefficient (upper left panel), particle extinction coefficient (upper right panel), particle lidar ratio (lower left panel) and particle linear depolarisation ratio (lower right panel) at 532 nm for the selected flight track south-west of Ireland on 14 May. The grey shaded areas mark the statistical error, the error bars the systematic errors.

ACPD
12, 26843–26869, 2012

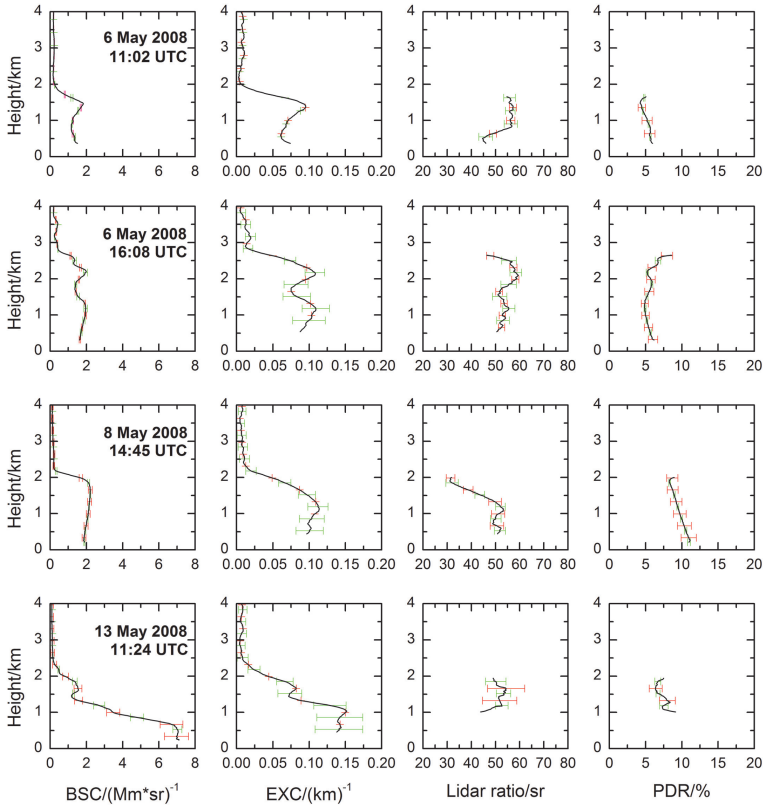

Fig. 7. Vertical profiles of backscatter coefficient (BSC), extinction coefficient (EXC), lidar ratio and particle linear depolarisation ratio (PDR) at 532 nm for selected measurement periods during the first half of the EUCAARI-LONGREX campaign. The red error bars indicate the systematic errors; the green error bars indicate the statistic errors.

ACPD
12, 26843–26869, 2012

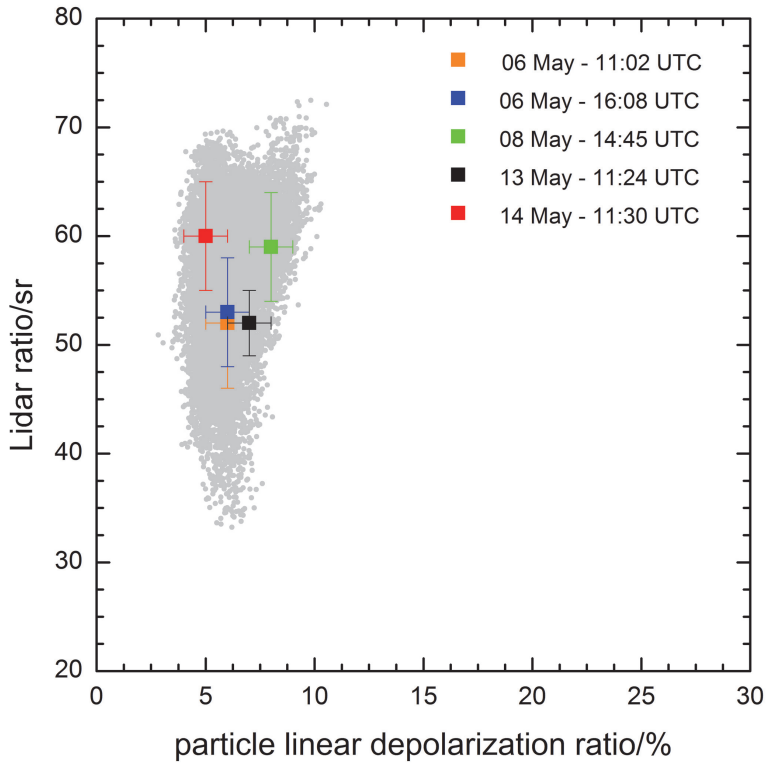

Fig. 8. Scatterplot of lidar ratio vs. particle linear depolarisation ratio (both at 532 nm) for measurements within pollution aerosol layers during the first half of the EUCAARI-LONGREX campaign. The grey dots show all lidar measurement points within pollution layers, the colour-coded squares show the mean values within the pollution layers of the vertical profiles presented in Figs. 6 and 7.

ACPD
12, 26843–26869, 2012

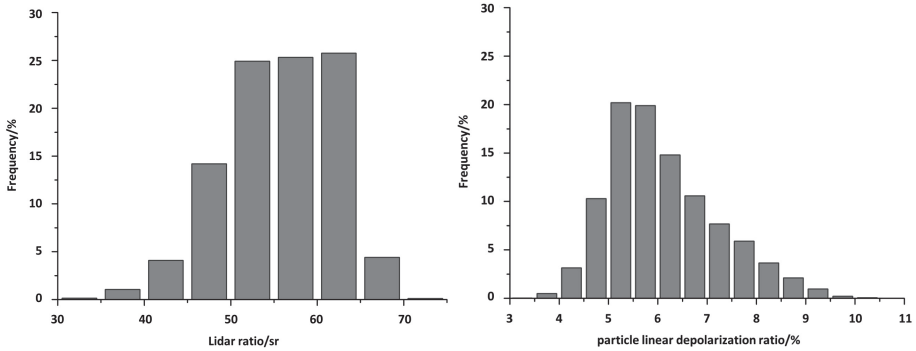

Fig. 9. Frequency distribution of the lidar ratio (left panel) and the particle linear depolarisation ratio (right panel) at 532 nm for all considered measurements during the first half of the EUCAARI-LONGREX campaign.

ACPD
12, 26843–26869, 2012

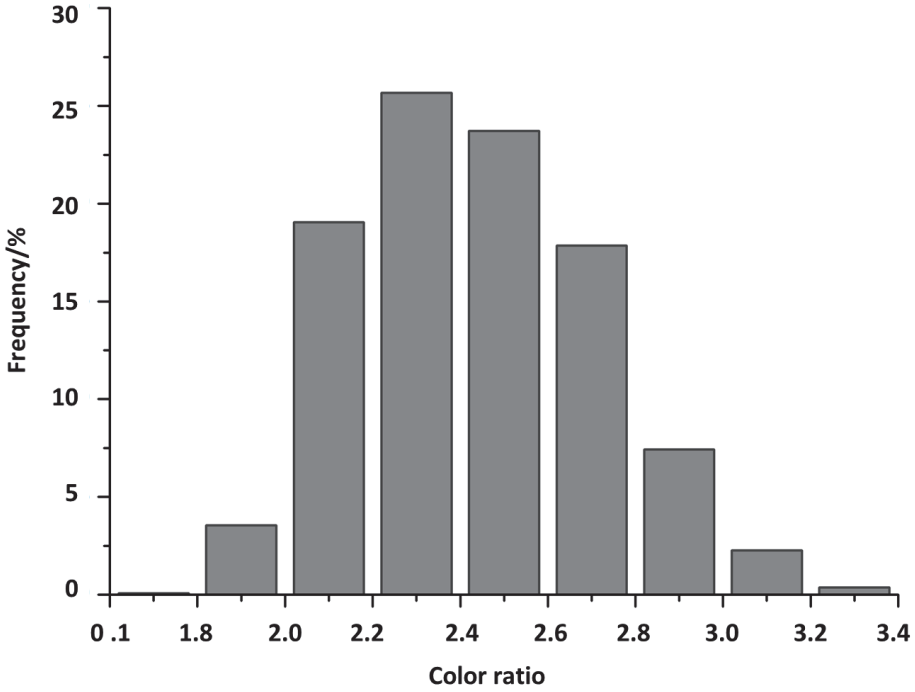

Fig. 10. Frequency distribution of the colour ratio for all considered measurements during the first half of the EUCAARI-LONGREX campaign.

ACPD
12, 26843–26869, 2012